Radiation Controls the Interannual Variability of Evaporation of a Subtropical Lake

Wei Xiao[1,2] , **Zhen Zhang[1]**, **Wei Wang[3]** , **Mi Zhang[1]**, **Qiang Liu[1,4]**, **Yongbo Hu[1]** , **Wenjing Huang[1]**, **Shoudong Liu[1]**, and **Xuhui Lee[5]**

[1]Yale-NUIST Center on Atmospheric Environment and Collaborative Innovation Center on Forecast and Evaluation of Meteorological Disasters, Nanjing University of Information Science and Technology, Nanjing, China, [2]NUIST-Wuxi Research Institute, Wuxi, China, [3]Jiangsu Key Laboratory of Agricultural Meteorology, Nanjing University of Information Science and Technology, Nanjing, China, [4]Binjiang College, Nanjing University of Information Science and Technology, Wuxi, China, [5]School of Forestry and Environmental Studies, Yale University, New Haven, CT, USA

Abstract Does lake evaporation increase or decrease under the scenario of climate warming? This paper aims to answer this question by investigating the controlling mechanism of interannual variations in lake evaporation at a subtropical lake. The research methodology is based on continuous eddy covariance measurement over >7 years and a diagnostic analysis using the surface energy balance principle. The results indicate that lake evaporation was enhanced mainly by increasing energy inputs including solar radiation and incoming longwave radiation and was weakened by surface feedback through outgoing longwave radiation. The incoming longwave radiation was positively correlated with cloud cover. Bowen ratio and surface albedo had slight effect on the change of lake evaporation. The annual lake evaporation can be predicted by the Priestly-Taylor model using a larger coefficient of 1.39 than the original value of 1.26, suggesting that advection or entrainment in the atmospheric boundary layer may play a role in lake evaporation.

1. Introduction

Evaporation (E) is a major output term of the water balance of a lake system. There is a pressing need for a predictive understanding of processes that control lake E in a changing climate (Friedrich et al., 2018; Hunter et al., 2015). Energy conservation requires that lake evaporation must satisfy the energy balance constraint. This constraint however manifests itself differently at different time scales, and the key drivers of E also depend on the time scale of interest. At short time scales (hourly to daily), lake E is controlled by wind speed u and vapor pressure difference (D) between the lake surface and the overlaying air (Blanken et al., 2000, 2011; Liu et al., 2009; T. Wang et al., 2017) and can be described using the turbulent mass transfer approach or the Dalton equation (Brutsaert, 1982; Garratt, 1994). Short-term fluctuations in u and D can cause substantial changes in E, even without changes in the solar energy input to the lake. A classic example is the large E pulse associated with rises in u and D during the passage of a cold front (Blanken et al., 2000; Liu et al., 2009, 2011). Here, the energy that fuels the increased E comes from the internal heat stored in the lake water. Another mechanism underlying E temporal dynamics is changes in energy allocation, such as a reduction in Bowen ratio, which allows more available energy to support E than the sensible heat flux (W. Wang et al., 2018). At the seasonal time scale, the monthly E follows closely the net radiation R_n but with a phase delay ranging from 1 month for shallow lakes (W. Wang et al., 2014; Zhao & Liu, 2018) to 5 months for deep lakes (Blanken et al., 2011), due to the buffering effect of heat storage of water. Lee et al. (2014) found that the monthly E during the open-water season can be predicted by the Priestley-Taylor (PT) model if the available energy, that is, R_n minus water heat storage change, is known. In high latitudes, ice phenology influences the lake evaporation with significant latent heat flux release during the freezing period and energy absorption during melting conditions due to latent heat of fusion associated with freezing and thawing (Franz et al., 2018; K. Xiao et al., 2018).

An outstanding question is whether the drivers at short time scales can be used to explain and predict variabilities of lake E at annual and longer time scales. Traditionally, researchers argue that nonenergy-related meteorological variables, such as wind speed, air temperature, and cloud amount, determine the long-term trends of lake E (e.g., Blanken et al., 2011; McJannet et al., 2013; K. Xiao et al., 2018). More recently,

W. Wang et al. (2018) proposed that changes in annual E can be interpreted as component contributions from energy inputs into the system (incoming shortwave and incoming longwave radiation) and from changes in energy allocation (Bowen ratio and albedo). The majority of the published papers on this topic use both nonenergy variables and energy variables to explain statistically historical lake E variations (Friedrich et al., 2018; Hu et al., 2017; Lazhu et al., 2016; Lenters et al., 2005). Such statistical approaches, while helpful in uncovering processes underlying E trends at a specific location, cannot be easily extended to other regions or be used for future predictions.

A hindrance to progress in the investigation of lake E is the lack of long-term observational data. The majority of the studies cited above either use pan evaporation data as a proxy for historical lake evaporation (e.g., Brutsaert & Parlange, 1998; Hu et al., 2017; Peterson et al., 1995) or rely on model-calculated lake water vapor flux (e.g., Feng et al., 2016; Guo et al., 2019; Ma et al., 2016; K. Xiao et al., 2018). One exception is the study of Lenters et al. (2005), who measured the evaporation of Sparkling Lake in northern Wisconsin, USA, using the energy budget method over a 10-year period from 1989 to 1998. In recent years, an increasing number of studies have deployed the eddy covariance technique to measure evaporation from lakes and reservoirs (e.g., Blanken et al., 2000, 2003; Bouin et al., 2012; Du et al., 2018; Liu et al., 2009; McGloin et al., 2015; Nordbo et al., 2011; Rouse et al., 2003; Tanny et al., 2011). Due to the difficulty of operation, the longest eddy covariance measurement so far has lasted 4 years with data gaps of several months (Du et al., 2018) or four ice-free seasons (Nordbo et al., 2011).

This study aims to characterize the interannual variability of lake evaporation and investigate the drivers of the variability. Results are based on continuous eddy covariance data collected at a shallow lake in the subtropical monsoon climate over a 7-year period (2011–2017). The study seeks to address three questions: (1) Is the interannual variation of lake evaporation caused by variation in radiation or in temperature? (2) Can the classic Priestley and Taylor (1972) model predict lake evaporation at the annual scale? (3) To what extent is the long-term trend of lake evaporation predictable?

2. Materials and Methods

2.1. Eddy Flux Site and Data

The lake evaporation observation was conducted at Lake Taihu, the third largest freshwater lake in China (area of 2,400 km^2 and mean depth of 1.9 m), as part of the Taihu Eddy Flux Network (Lee et al., 2014). The network consists of seven eddy flux sites in the lake and one site on land (Figure S1 in the supporting information). In this study, we combined measurements from two lake sites (site IDs MLW and BFG) to form continuous half-hourly time series of the lake latent heat flux and other meteorological and flux variables from July 2010 to December 2017. Data collection at MLW (31°25′N, 120°13′E), located about 200 m near the north shore of the lake, started in June 2010. The eddy covariance system (an open-path infrared gas analyzer [model LI7500, Li-Cor, Inc., Lincoln, Nebraska, USA] and a three-dimensional sonic anemometer/thermometer [model CSAT3, Campbell Scientific, Inc., Logan, UT, USA]) was mounted on a concrete pillar, at a measurement height of 3.5 m above the water surface (W. Xiao et al., 2013). The radiation components were measured with a net radiometer (model CNR4, Kipp & Zonen B.V., Delft, The Netherlands) mounted at a height of 3.7 m above water surface. According to a footprint analysis, the largest contribution to the observed flux occurred at a distance of 88, 27, and 207 m away from the EC instrument under neutral, unstable, and stable conditions, respectively (Wang et al., 2014). Stable stability (pp. 953–1028) occurred less than 7% of the observations at MLW.

BFG (31°10′N, 120°24′E) is a site located in the eastern portion of the lake with open fetch (>4 km in all directions). The eddy covariance system (an open-path gas analyzer [model EC150, Campbell Scientific, Inc.] and a CSAT3 sonic anemometer/thermometer) was mounted on a fixed platform, and the measurement height was 8.5 m above the water surface (Lee et al., 2014). The radiometer was of the same type as MLW and mounted at a height of 3.0 m above the water surface. Its data collection started in December 2011 and has continued more or less uninterrupted since then.

For the composite data presented in this study, measurements made at MLW were used for the period from July 2010 to December 2011, and measurements at the BFG site for the period from January 2012 to December 2017. According to Wang et al. (2014), the monthly mean evaporation flux and the associated

driving variables have negligible spatial variations across the whole lake, so the MLW data were included here to extend the data period for a better trend detection. But mindful of the site change, we did not use the MLW data in the attribution analysis presented below.

Standard eddy covariance correction, quality control, and gap filling procedures were applied. Coordinate rotation (Lee et al., 2004) and density corrections (Lee & Massman, 2011; Webb et al., 1980) were performed on the latent heat flux measurement. Data were filtered to remove rain interference and instrument malfunctions. All the time series were gap filled. Small gaps shorter than 2.5 hr were filled using linear interpolation. Bigger gaps were filled using the data from the other eddy covariance sites according to the following procedure. First, a linear regression was made for a variable to be gap filled, using valid observations at MLW or BFG and those at the other lake sites during the month when the gap occurred. Next, the data from the site with the highest correlation were used to fill the data gap at MLW or BFG. During persistent rainstorms, the eddy flux observations became unreliable from all the lake eddy covariance sites; in such cases, gaps in the latent heat flux and sensible heat flux were filled with locally calibrated bulk transfer relationships (Xiao et al., 2013). The fraction of the gaps is about 29%.

The complete half-hourly time series include lake latent and sensible heat fluxes (without energy balance adjustment), the four components of the radiation balance, and micrometeorological variables (air temperature and water vapor pressure; see supporting information). For monthly and annual latent and sensible heat fluxes, energy balance closure was forced at the time step of 1 month, and the energy balance ratio (the ratio of the sum of sensible and latent heat flux to the available energy) was 0.68. Mechanisms that control lake evaporation are based on the energy balance principle. To be consistent with this theoretical underpinning, it is a standard practice in micrometeorology to adjust sensible and latent heat fluxes so that the energy is balanced (Blanken et al., 1997; Twine et al., 2000). The implicit assumption is that the energy missed by the eddy covariance technique, such as that associated with horizontal and vertical advection, can be reallocated to the eddy fluxes in proportion according to the measured Bowen ratio.

The heat storage change (G) was calculated from the temporal variation of depth-weighted average temperature of the water column (Blanken et al., 2000). The water column was divided to five layers (0–0.20, 0.20–0.50, 0.50–1.00, 1.00–1.50, and 1.50 m to sediment). The lake surface temperature was derived from the incoming and outgoing longwave radiation observation. Water temperature at 0.20-, 0.50-, 1.00-, and 1.50-m depth and sediment temperature were measured using temperature probes (model 109-L, Campbell Scientific, Inc., Logan, UT, USA). The monthly G value ranged from about 20 W m^{-2} in June to −20 W m^{-2} in November, comparable to the values reported by W. Wang et al. (2014). According to Wang et al. (2014), the monthly G agreed well between MLW and BFG, indicating the robustness of the estimation method.

A potential source of error in the energy balance adjustment was associated with the heat storage term G. In deep lakes, the G term is difficult to obtain because temperature profile measurements are typically restricted to the surface water layer. In our study, the profile measurement spanned the whole water column (0- to 2-m depth). However, our procedure omitted the heat exchange between the water column and the sediment beneath it. To obtain a sense of the sediment flux, we ran a locally tuned version of the lake simulator CLM4-LISSS (Deng et al., 2013; Subin et al., 2012) using the meteorological observations over the full experimental period. We also estimated the sediment heat flux using the method described by Wang and Bras (1999). This method builds the relationship between the heat flux conducted into the soil and the time series of sediment temperature at hourly time resolutions. In our calculation, we assumed a thermal conductivity of 3.436×10^6 J m^{-3} K^{-1} to represent saturated mineral soil with a porosity of 0.36. The results from both the CLM4-LISS model and the Wang procedure indicate that the monthly sediment flux was too small to be consequential (−0.25 W m^{-2} in mid-winter to 0.24 W m^{-2} in mid-summer; positive value indicating heat flux into the sediment).

2.2. Ancillary Meteorological Data

To analyze the effect of meteorological variables on lake evaporation, cloud cover data were obtained from China Meteorological Data Service Center (http://data.cma.cn/data/). Cloud cover data at four weather stations around Lake Taihu were used, including Liyang (site ID 58345, 31.26°N, 119.29°E, 6 m above sea level) to the west, Wuxi (site ID 58354, 31.37°N, 120.21°E, 3 m above sea level) to the north, Dongshan (site ID

58358, 31.04°N, 120.26°E, 17 m above sea level) to the east, and Huzhou (site ID 58450, 30.52°N, 120.03°E, 7 m above sea level) to the south (Figure S1). To minimize the effect of spatial variations, we used the mean value of cloud cover from the four sites to represent the condition over Lake Taihu. This spatial mean C value was highly correlated with the annual incoming longwave radiation observed over the lake (linear correlation of 0.84, $p < 0.05$; Figure S4a), supporting the use of the mean C as an indicator of sky conditions over the lake.

The wind speed observation at MLW was made at a lower height (3.5 m above the water surface) than at BFG (8.5 m above the water surface). Because wind speed is highly sensitive to measurement height, the MLW wind speed is not suitable for time change analysis. Instead, we used a regression method to estimate the wind speed over the lake in 2011. We first established a linear regression of the annual mean wind speed at BFG with that at the Dongshan weather station, the station closest to the BFG site (linear distance of 10.43 km). We then used the regression to estimate the lake mean wind speed in 2011.

2.3. Analytical Frameworks

We use two analytical frameworks to develop a predictive understanding of interannual variations of the lake E. The first one is the classic PT model of evaporation. The model expresses the lake latent heat flux as

$$\lambda E = \alpha \frac{s}{s + \gamma}(R_n - G),\tag{1}$$

where λ is latent heat of vaporization of water, s is the slope of the saturated vapor pressure–temperature curve, γ is psychrometric constant, and α is the PT constant with a default value of 1.26 (Priestley & Taylor, 1972).

According to the PT model, the lake Bowen ratio is related to α as

$$\beta = \frac{1}{\alpha} + \frac{\gamma}{\alpha s} - 1.\tag{2}$$

According to equation 2, β is a function of temperature, decreasing from 1.0 at 0 °C to 0.08 at 25 °C.

The second framework allows attribution of the interannual variability of lake evaporation to contributions by individual drivers. Using the surface energy balance constraint, Wang et al. (2018) express the change in the lake latent heat flux as contributions of changes in Bowen ratio (β), albedo (a), incoming solar radiation ($K_\downarrow$), incoming longwave radiation ($L_\downarrow$), outgoing longwave radiation $L_\uparrow$, and heat storage G:

$$\Delta(\lambda E) = -\frac{R_n - G}{(1 + \beta)^2}\Delta\beta - \frac{K_\downarrow}{1 + \beta}\Delta a + \frac{1}{1 + \beta}[(1 - a)\Delta K_\downarrow + \Delta L_\downarrow - \Delta L_\uparrow] - \frac{1}{1 + \beta}\Delta G,\tag{3}$$

where R_n is the surface net radiation. Similar energy balance attribution analyses have been reported by Lee et al. (2011), Richter and Xie (2008), and Roderick and Farquhar (2002). Here we applied equation 3 to diagnose drivers of the observed interannual changes in lake E. In this analysis, Δ denotes changes of the annual mean value in 2013 to 2017 relative to the annual mean value in 2012. Because the annual mean value of water heat storage change in Lake Taihu was close to 0, the last term in the above equation was ignored in this study. Data in 2011 were not used in the attribution analysis to avoid the systematic bias caused by the lake surface albedo change due to site switching (the albedo was 0.03 lower at MLW than at BFG). Year 2012 was used as the baseline year because the annual lake E was the lowest among the six full observational years (2012–2017) at BFG.

3. Results

3.1. Interannual Trends of Environmental Variables

Interannual variabilities for meteorological variables and radiation budgets are shown in Figures S2 and S3 and Tables S1 and S2. During the period of 2011–2017, the annual mean air temperature (T_a) showed a significantly increasing trend, with a regression slope of 0.20 °C year^{-1} and $R^2 = 0.76$ between T_a and year and a range of 16.2 to 17.6 °C. Cloud cover (C) increased significantly, with $R^2 = 0.76$ and the minimum and

maximum values of 45% and 66% in 2013 and 2016, respectively. The incoming longwave radiation ($L_\downarrow$) also showed an increasing trend, at a rate of 1.7 W m^{-2} year^{-1} ($R^2 = 0.83$). The outgoing longwave radiation increased from 404.0 W m^{-2} in 2011 to 411.9 W m^{-2} in 2017. No clear interannual trends were found for atmospheric vapor pressure (e_a), wind speed (u), incoming shortwave radiation ($K_\downarrow$), lake surface albedo (a), and the fraction of diffuse radiation to solar radiation.

The correlation between the annual mean $L_\downarrow$ and $K_\downarrow$ with meteorological variables is shown in Figure S4. A positive correlation was observed between $L_\downarrow$ and T_a (linear correlation coefficient $r = 0.84$, $p < 0.05$), e_a ($r = 0.77$, $p < 0.05$), and C ($r = 0.77$, $p < 0.05$). A three-variable linear regression yielded the equation

$$L_\downarrow = 315 \, (\pm 104) - 0.135 \, (\pm 9.58) \times T_a + 2.10 \, (\pm 4.33) \times e_a + 0.280 \, (\pm 0.289) \times C, \tag{4}$$

with $R^2 = 0.91$ and $p < 0.05$. If T_a was ignored, the linear regression equation became

$$L_\downarrow = 315 \, (\pm 26.9) + 2.05 \, (\pm 1.81) \times e_a + 0.279 \, (\pm 0.201) \times C, \tag{5}$$

with $R^2 = 0.91$ and $p < 0.01$. In these two equations, T_a is in the unit of °C, e_a in hPa, and C in percentage, and parameter bounds are 95% confidence intervals. The results suggest that the interannual variability of $L_\downarrow$ was driven primarily by e_a and C. The two-variable linear correlation performed better than the single variable regression with either e_a or C. In comparison, the correlation of $K_\downarrow$ with the meteorological variables was not statistically significant, even though it showed a slight increasing trend with increasing T_a and e_a and with decreasing C.

3.2. Seasonal and Interannual Variabilities in Lake Evaporation

The time series data on monthly and annual latent heat flux λE are given in Figure 1 and Table S1. A slight increasing trend in the annual lake evaporation was observed, at a rate of 1.2 ± 1.9 W m^{-2} year^{-1} ($R^2 = 0.25$, $p = 0.14$). The λE was lowest in 2011, with a mean value of 76.1 W m^{-2}, equivalent to 974 mm year^{-1} of lake evaporation. It increased to a higher value of 87.4 W m^{-2} (1120 mm year^{-1}) in 2013 and then decreased to a lower value in 2014. From 2014 to 2017, λE increased consistently, from 78.7 to 87.2 W m^{-2} (1,008 to 1,118 mm year^{-1}).

A strong seasonal variability was observed in each year. The lake evaporation was high in the summer and low in the winter. The peak value usually occurred in July or August except for 2014 when the lake evaporation was weak in summer (peak value in May). The mean value of λE over the seven summers (from June to August 2011 to 2017) was 128.7 W m^{-2}, which is about four times of the mean value over the seven winters (from December to the next February, December 2010 to February 2017, 31.6 W m^{-2}). The winter λE varied only slightly between years, with the winter mean value ranging from 25.0 W m^{-2} (December 2012 to February 2013) to 36.9 W m^{-2} (December 2016 to February 2017). But the peak monthly value in the summer varied substantially, from the lowest of 117.5 W m^{-2} in July 2011 to the highest of 222.5 W m^{-2} in August 2016. In other words, the interannual variability in the lake E was primarily related to the summer time variability.

The relationships between the annual λE with energy terms and nonenergy meteorological variables are shown in Figure 2. Regarding the radiation terms, the annual λE was significantly correlated with $K_\downarrow$ ($r = 0.87$, $p < 0.05$); in other words, lake evaporation was enhanced when incoming shortwave radiation was strong. Generally, λE was higher when $L_\downarrow$ was high or β was low, even though the correlations are not statistically significant. Among the nonenergy terms, lake evaporation was positively correlated with T_a ($r = 0.89$ and $p < 0.01$) and with e_a ($r = 0.75$, $p = 0.05$) and was not correlated with wind speed ($r = -0.06$, $p = 0.89$).

3.3. Comparison With the PT Model Prediction

The λE calculated by the PT model is compared with the observation at the monthly and annual scales (Figure 3). At the monthly scale, the calculated λE using the default α agreed well with the observation if all the monthly data during the 7-year period were considered. If each season is analyzed individually, forcing good agreement requires smaller α values for the summer and the fall seasons (1.23 and 1.30, respectively) and higher values for the spring and the winter seasons (1.36 and 1.60, respectively; Figure S5). At
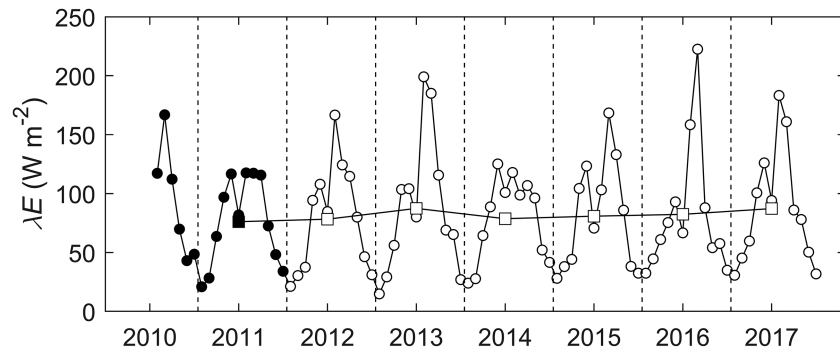
Figure 1. Time series of monthly and annual λE at Lake Taihu. Circles and squares denote monthly and annual means, respectively. Filled symbols denote observations at MLW.
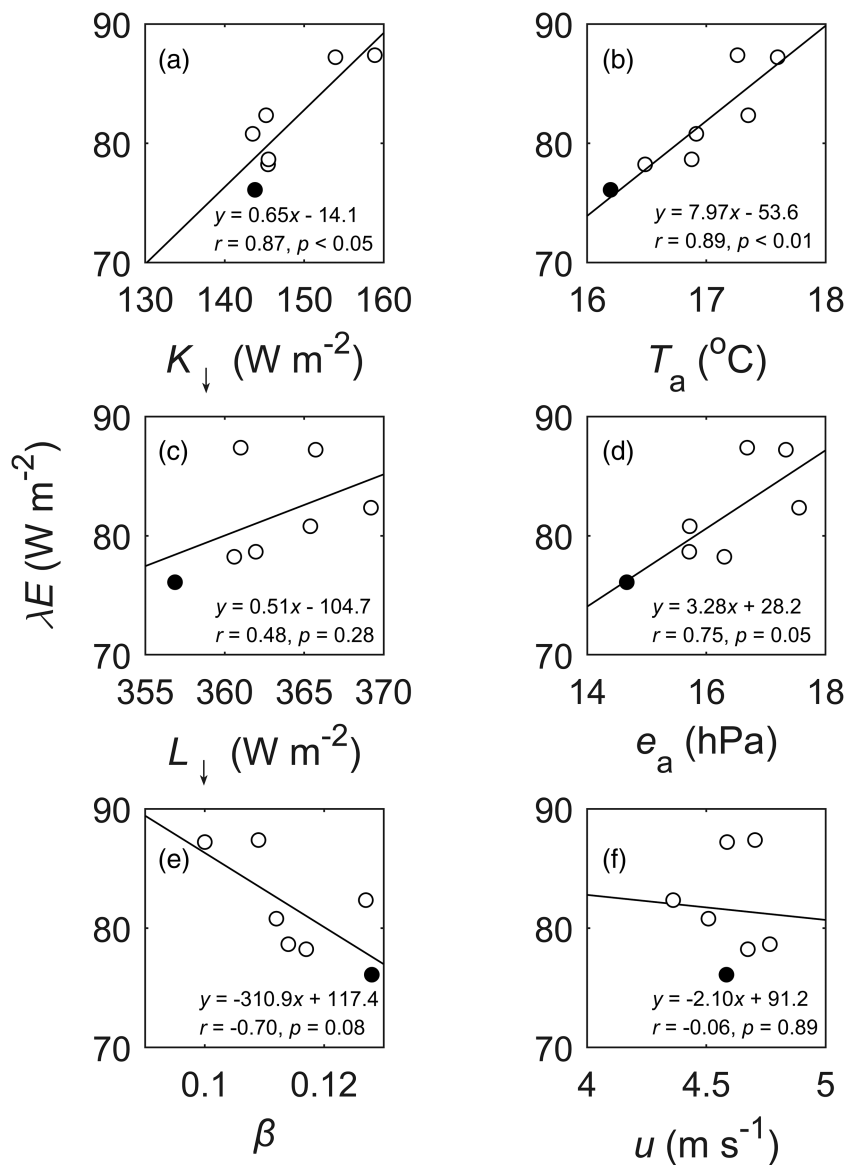

Figure 2. Correlation of annual latent heat flux with energy terms (left panels, a: incoming shortwave radiation; c: incoming longwave radiation; and e: Bowen ratio) and nonenergy variables (right panels, b: air temperature; d: atmospheric vapor pressure; and f: wind speed). Filled symbols denote observations at MLW.
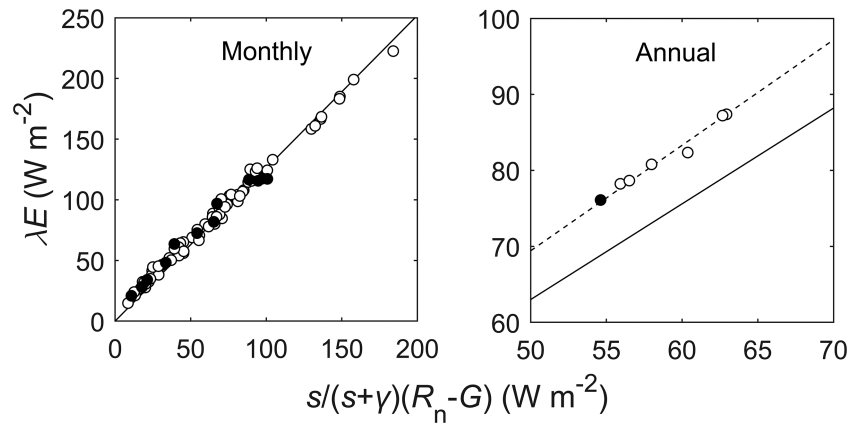
Figure 3. Latent heat flux λE as a function of $s/(s + \gamma)(R_n - G)$. Circles denote observations, and solid and dashed lines represent slopes of 1.26 and 1.39, respectively. Filled symbols denote observations at MLW.

the annual scale, the default α value did not work anymore, and a systematic low bias in the calculated λE was evident. The optimal α value should be 1.39 according to the annual data.

The monthly tuned α showed statistically significant and negative correlation with the saturation vapor pressure deficit (D) and temperature (Figures 4a and 4b; $p < 0.001$) but without significant correlation with D/s (Figure 4c; $p = 0.069$). A moderate correlation was also found with wind speed (Figure S6, $p < 0.05$). The annual composite α showed a U pattern from January to December, with a peak value of 1.63 in December and the lowest value of 1.22 in August (Figure S7). The seasonality of α mirrors the seasonal patterns of D and temperature (Figure S7).

3.4. Attribution of Annual Lake Evaporation Change

The results of energy balance attribution of the latent heat flux change are shown in Figure 5. The changes in latent heat flux ($\Delta\lambda E$) and energy balance components were calculated in reference to the values in 2012 (Table 1). The intermediate variables used in this calculation are given in Table S1. In all, there is a total of five annual change calculations. The results are plotted for individual years (Figure 5a). Generally, the contribution of $\Delta\beta$ to $\Delta\lambda E$ was relatively small, ranging from -0.7 to 1.4 W m^{-2}. Surface albedo had consistently positive contributions to $\Delta\lambda E$, ranging from 0.9 to 2.4 W m^{-2}. Contributions from the incoming solar radiation change $\frac{1}{1+\beta}[(1-a)\Delta K_\downarrow]$ and incoming longwave radiation change $\frac{1}{1+\beta}[\Delta L_\downarrow]$ to $\Delta\lambda E$ (equation 3) varied between -1.6 and 11.1 W m^{-2} and between 0.4 and 7.6 W m^{-2}, respectively.

Figure 5b shows the mean component contributions to $\Delta\lambda E$ from the 5 years (2013–2017, all in reference to 2012). On average, the major positive contributions came from $\Delta L_\downarrow$ (3.6 ± 2.6 W m^{-2}) and $\Delta K_\downarrow$ (3.3 ± 4.9 W m^{-2}). About half of these were offset by the surface feedback or changes in the outgoing longwave radiation ($\Delta L_\uparrow$) due to warming of the water surface (-3.8 ± 1.4 W m^{-2}) (note that these values are contributions from the change terms according to equation 3 and are different from the change terms themselves).

4. Discussion

4.1. The Dominant Role of Energy Inputs

The attribution analysis indicates that energy inputs ($L_\downarrow$ and $K_\downarrow$) to the lake played a dominant role in the interannual variability the lake evaporation (Figure 5). The incoming longwave radiation was higher from 2013 to 2017 than in 2012 and played a positive role in enhancing lake evaporation, especially when $\Delta\lambda E$ was moderate (2014 and 2015). The highest annual lake evaporation occurred in 2013; during the same year, the incoming shortwave radiation was the highest (Table S1).

Statistical analysis supports the conclusion that it was the energy inputs instead of nonenergy forcing variables that drove the observed interannual variability in the lake evaporation. In a single variable correlation analysis, the annual E was correlated with three energy variables (β, $L_\downarrow$, and $K_\downarrow$; Figure 2, left panels) and two
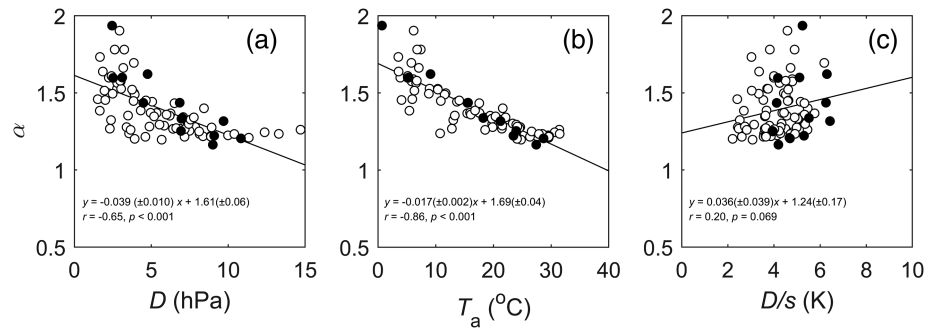
Figure 4. The Priestley-Taylor coefficient versus vapor pressure deficit (a), air temperature (b), and the ratio of vapor pressure deficit to the slope of the saturation vapor pressure curve D/s (c) for each month from 2011 to 2017. Filled symbols denote observations at MLW.

nonenergy variables (T_a and e_a). Based on such correlation patterns, it would be tempting to conclude that energy and nonenergy variables had played equal roles in regulating the lake E. However, in a stepwise multivariable linear regression between annual λE and annual T_a, β, e_a, $L_\downarrow$, and $K_\downarrow$, only $L_\downarrow$ and $K_\downarrow$ remained as significant predictors. The resulting regression equation is

$$\lambda E = -198.2\,(\pm 28.5) + 0.508\,(\pm 0.076)\,L_\downarrow + 0.644\,(\pm 0.052)\,K_\downarrow\,\left(R^2 = 0.97,\ p < 0.001,\ n = 7\right). \quad (6)$$

The regression result indicates that energy inputs were the main control of interannual variability of lake evaporation, while nonenergy terms including air temperature and atmospheric vapor pressure had minor effects. Change in energy allocation via Bowen ratio was a minor contributor (Figure 5) despite appreciable interannual variability in air temperature (Table S2). This is because lake Bowen ratio in subtropical climates is not sensitive to temperature (Wang et al., 2018).
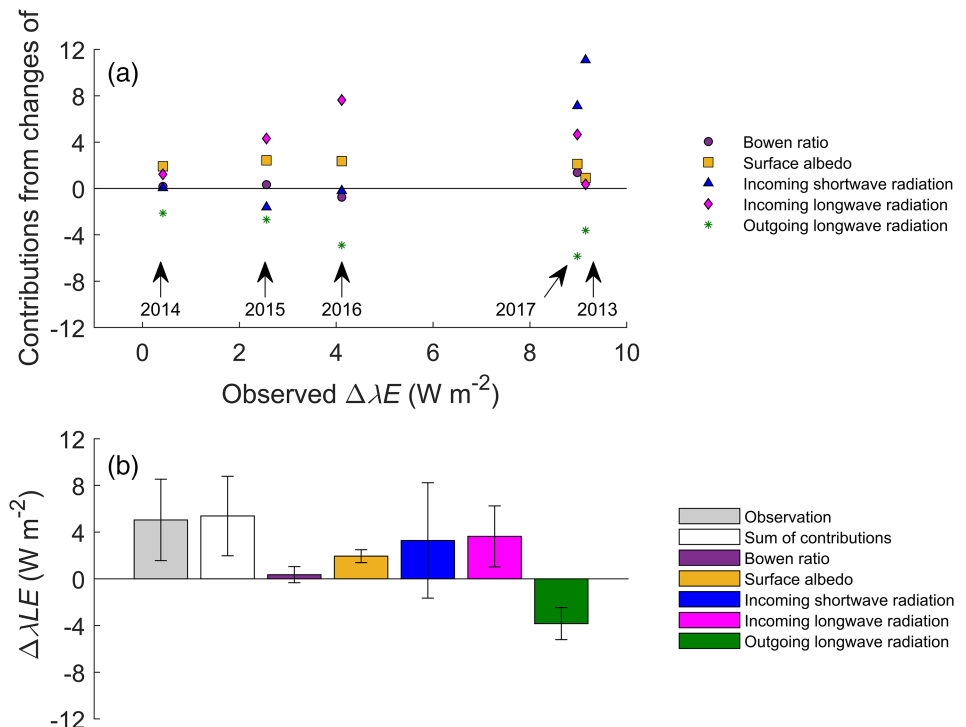

Figure 5. Attribution of the annual lake evaporation change $\Delta\lambda E$. (a) Results for individual years from 2013 to 2017. (b) Multiyear means. Error bars are ±one standard deviation.

Table 1
Changes of Latent Heat Flux (Λe), Incoming Solar Radiation ($K_\downarrow$), Incoming Longwave Radiation ($L_\downarrow$), Outgoing Longwave Radiation ($L_\uparrow$), Net Radiation (R_n), Surface Albedo (α), Bowen Ratio (β), Air Temperature (T_a), and Water Vapor Pressure (e_a) in Reference to Their Respective Values Observed in 2012

	$\Delta\lambda E$ (W m^{-2})	$\Delta K_\downarrow$ (W m^{-2})	$\Delta L_\downarrow$ (W m^{-2})	$\Delta L_\uparrow$ (W m^{-2})	ΔR_n (W m^{-2})	$\Delta\alpha$	$\Delta\beta$	ΔT_a (°C)	Δe_a (hPa)
2011	−2.1	−1.6	−3.7	−1.5	−0.2	−0.024	0.011	−0.3	−0.16
2013	9.1	13.4	0.4	4.0	9.6	−0.006	−0.008	0.8	0.04
2014	0.4	0.1	1.4	2.4	1.2	−0.015	−0.002	0.4	−0.06
2015	2.6	−1.9	4.8	3.0	2.7	−0.019	−0.005	0.4	−0.06
2016	4.1	−0.2	8.6	5.5	5.5	−0.018	0.010	0.9	0.13
2017	9.0	8.5	5.1	6.4	8.7	−0.015	−0.017	1.1	0.10
Average	5.0	4.0	4.1	4.3	5.5	−0.015	−0.002	0.7	0.03
Standard deviation	3.5	6.0	2.9	1.5	3.3	0.004	0.010	0.3	0.08

Our results agree with the long-term observation by Lenters et al. (2005) for Sparking Lake in northern Wisconsin, USA. These authors found that interannual variations in the lake E are attributed mainly to changes in net radiation and moderately to variations in temperature and humidity.

4.2. PT Model Performance

A number of studies have reported the performance of the PT model at subday time scales (Assouline et al., 2016; Bello & Smith, 1990; X. Guo et al., 2015; Stewart & Rouse, 1976). In the present study, the focus is annual evaporation. The PT model, when applied at the annual time scale, underestimated the lake evaporation by 9.3% (Figure 3). Forcing agreement with the observation requires that the model coefficient be increased from the original value of 1.26 to 1.39 (Figure 3). Similarly, W. Wang et al. (2018) reported that the annual lake E predicted by the original PT model is biased low in comparison with the E calculated by a lake simulator imbedded in the Community Land Model. They found an optimized coefficient of 1.31 for global lakes.

The original PT coefficient was based on observations at subday time scales (Priestley & Taylor, 1972). Since the slope of the vapor saturation curve (s) is a nonlinear function of temperature, strictly, the PT model should be applied at shorter time steps instead using the annual mean temperature (as was done in Figure 3) to avoid nonlinear errors. Figure 6 shows three additional sets of PT model calculation. In the first set, the PT model with the original coefficient was applied at the daily time step using the observed daily mean temperature and available energy, and the calculated daily latent heat flux was summed over the annual period to give the annual flux. The second set was identical to the first set except that the calculation was done at the monthly time step. In the third set, the calculation was also done at the monthly time step, but the coefficient was a temperature-dependent function (Figure 4b). The PT model performance was not improved at the daily and monthly time steps, suggesting that temperature nonlinearity is not the main source of the model bias errors. By changing the PT coefficient either to a constant value of 1.39 at the annual time step or to a temperature-dependent function at the monthly time step, the model achieved near-perfect agreement with the observed annual evaporation.

We caution that the daily calculation may be more uncertain than the monthly and annual calculations because of errors in the lake heat storage G at the daily time step. The daily G values were relatively large in magnitude (25-percentile and 75-percentile values of −31 and 41 W m^{-2}, respectively) in comparison to the daily R_n (25-percentile and 75-percentile values of 34 and 145 W m^{-2}, respectively). Some of the deviations from the 1:1 line in Figure 6a could be caused by errors in G, such as those associated with disturbances by air turbulence to the water temperature profile (Nordbo et al., 2011).

Theoretically, α is bounded by a lower limit of unity. This limit corresponds to the situation where the saturation vapor pressure deficit D is 0 and therefore, evaporation occurs at the equilibrium rate (Monteith & Unsworth, 1990). As D increases, E will be greater than the equilibrium rate, and α will increase. However, the negative correlation between the observed α and D (Figure 4a) seems to contradict this theoretical expectation. This paradoxical behavior can be understood with the Penman-Monteith equation for saturated surfaces:
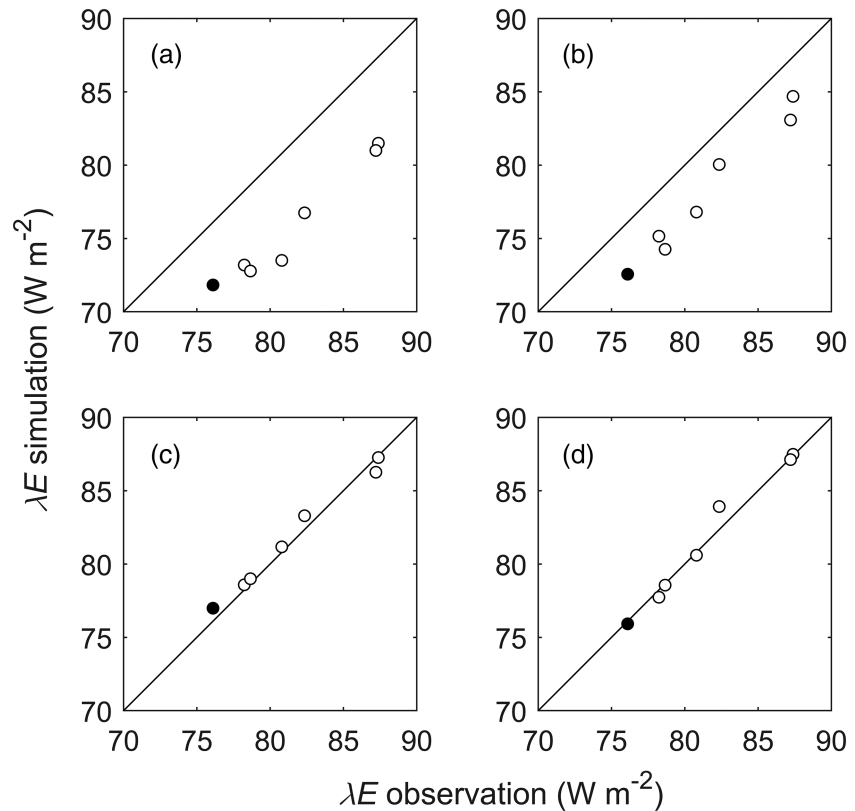
Figure 6. Observed annual λE versus annual λE calculated by four Priestley-Taylor procedures. (a) PT with original coefficient applied at the daily time scale; (b) PT with original coefficient applied at the monthly time scale; (c) PT with a temperature-dependent coefficient $\alpha = -0.017T_a + 1.69$ applied at the monthly time scale; (d) PT with tuned coefficient (1.39) applied at the annual time scale. Filled symbols denote observations at MLW.

$$\lambda E = \frac{s}{s+\gamma}\left[(R_n - G) + \frac{\rho c_p}{r_a}\frac{D}{s}\right], \tag{7}$$

where ρ represents air density, c_p is specific heat at constant pressure, and r_a is aerodynamic resistance. The second term on the right-hand side of the equation, commonly interpreted as the contribution of energy advection to lake evaporation, is the reason for the larger-than-unity α. If all other parameters remained constant, equation 7 shows that α would increase with increasing D. However, in the current study, D and temperature were correlated: D was higher in months with higher temperatures (and higher s values). Equation 7 suggests that the ratio D/s may be a better measure of the advective influence than D alone because the former considers both D and temperature. The results show a slight positive correlation of monthly α with D/s, increasing from 1.28 at $D/s = 2$ K to 1.50 at 6.5 K (Figure 4c).

The E underestimation by the original PT model was more severe in the cold season than in the warm season (Figure S5), consistent with the fact that the tuned α showed larger positive deviations from the original value at lower temperatures (Figure S5d). Similar seasonal behaviors were reported by de Bruin and Keijman (1979) and Gallego-Elvira et al. (2010). At present, the mechanism underlying this seasonal temperature dependence is unclear. A mathematical explanation, offered by de Bruin and Keijman (1979), is that the linear relationship between the actual E and the equilibrium E has a positive offset. Alternatively, α would increase with decreasing temperature if the Bowen ratio remained unchanged across seasons according to equation 2 (Gallego-Elvira et al., 2010), although in the present study, the Bowen ratio displayed a strong seasonality with the highest monthly value of 0.31 in February and the lowest monthly value of 0.05 in July (Figure S8). Regardless of the underlying mechanism, the temperature dependence based on seasonal variations (Figure 4b) should not be used to predict interannual and geographic variations in lake E

(Woolway et al., 2018). A recent study on ocean evaporation suggests that the PT relation has an internal inconsistency between surface temperature, radiation, and evaporation (Yang & Roderick, 2018).

4.3. Future Predictions

In the above analysis, equation 3 was used in a diagnostic mode to help us understand driving mechanism of the interannual variability in the observed lake E. This equation also provides a framework for making prediction on how E may change in response to climate change. Since an unambiguous result of rising CO_2 is rising air temperature, it is instructive to quantify how each of the terms in equation 3 may change in response to changes in air temperature ΔT_a.

According to the Bowen ratio formulation from the PT model (equation 2), the Bowen ratio change is negatively proportional to temperature change. The relationship is given by

$$\Delta\beta = -\left(\frac{\gamma}{\alpha s^2}\frac{ds}{dT_a}\right)\Delta T_a. \tag{8}$$

At the mean temperature of 290.1 K in the present study, the above equation gives a linear slope of $-0.022\ \mathrm{K}^{-1}$ with tuned annual α of 1.39. The decreasing trend of Bowen ratio with increasing surface temperature has been verified by theoretical and observational investigations (Assouline et al., 2016; X. Guo et al., 2015; Priestley & Taylor, 1972; Yang & Roderick, 2018).

The relationship between changes in outgoing longwave radiation and ΔT_a can be approximated by differentiation of the Stephan-Boltzmann law as

$$\Delta L_\uparrow = 4\sigma T_s^3 \Delta T_s \approx 4\sigma T_a^3 \Delta T_a, \tag{9}$$

where the lake surface temperature T_s is approximated by the air temperature T_a and σ is the Stephan-Boltzmann constant. This equation predicts a slope value of 5.5 W m^{-2} K^{-1} for the linear relationship between ΔT_a and $\Delta L_\uparrow$.

The incoming longwave radiation $L_\downarrow$ can be parameterized as

$$L_\downarrow = \epsilon_a \sigma T_a^4, \tag{10}$$

where ϵ_a is apparent atmospheric emissivity. The change in $L_\downarrow$ in response to ΔT_a is then given by

$$\Delta L_\downarrow = \left(4\epsilon_a \sigma T_a^3 + \sigma T_a^4 \frac{d\epsilon_a}{dT}\right)\Delta T_a. \tag{11}$$

Here, we use the Brutsaert (1975) clear-sky formula for ϵ_a:

$$\epsilon_a = 1.24(e_a/T_a)^{1/7}, \tag{12}$$

where e_a is atmospheric vapor pressure. We further assume that relative humidity is not sensitive to changes in T_a, or in other words, we assume that changes in e_a are driven primarily by changes in the saturation vapor pressure. With this assumption, we have

$$\frac{d\epsilon_a}{dT_a} = \frac{1}{7}\epsilon_a\left(\frac{RH}{e_a}s - \frac{1}{T_a}\right), \tag{13}$$

where RH is relative humidity in fraction. Equation 13 is combined with equations 12 and 11 to obtain a linear relationship between ΔT_a and $\Delta L_\downarrow$. For the conditions in the present study (mean RH = 0.84, mean e_a = 16.3 hPa, mean T_a = 290.1 K), the slope of this relationship is 7.4 W m^{-2} K^{-1}.

The performance of equations 8, 9, and 11 is shown in Figures 7a to Figure 7c. Once again, all the change terms are relative to their respective values observed in 2012. Except for the Bowen ratio change in 2016, these equations captured the observations reasonably well. The prediction of $\Delta L_\downarrow$ based on Brutsaert's emissivity formula is especially worthy noting because equation 12 is a parameterization for clear-sky conditions.
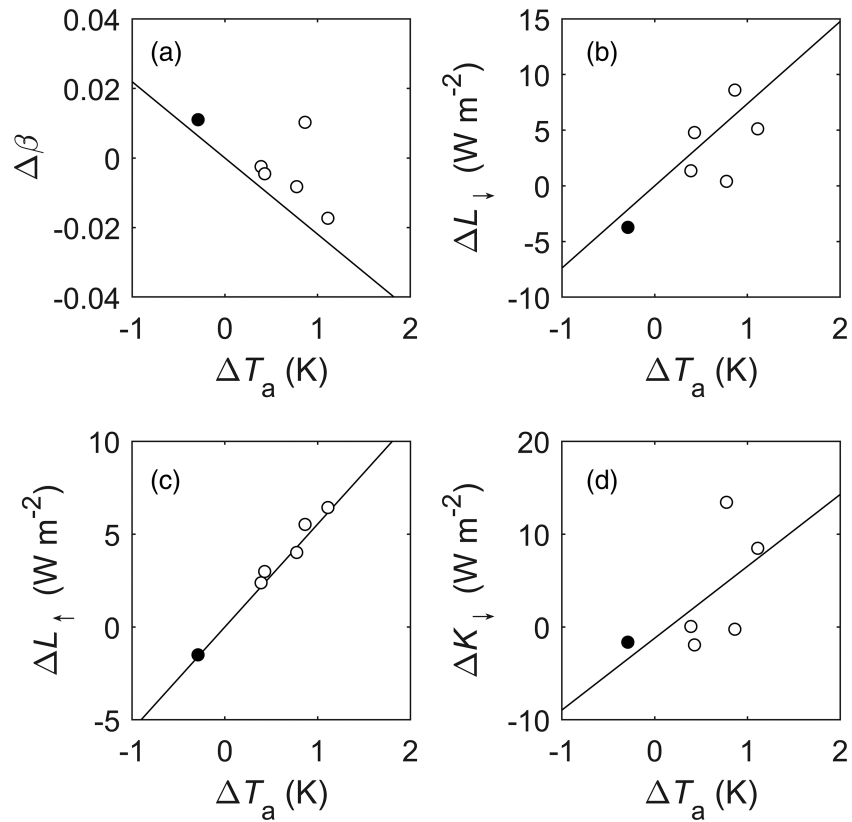
Figure 7. Comparison of observed (dots) and predicted (lines) temperature responses: (a) Bowen ratio change $\Delta\beta$ versus temperature change ΔT_a; (b) incoming longwave radiation change $\Delta L_\downarrow$ versus ΔT_a; and (c) outgoing longwave radiation change $\Delta L_\uparrow$ versus ΔT_a. Also shown is the relationship between the observed incoming shortwave radiation changes $\Delta K_\downarrow$ versus ΔT_a (panel d, with the regression line shown). Filled symbols denote observations at MLW.

The good performance of equation 11 suggests that the water vapor amount in the atmosphere dominated over cloudiness in controlling interannual variability in $L_\downarrow$. The remarkable agreement between $\Delta L_\uparrow$ and the Stephan-Boltzmann law prediction (Figure 7c) confirms that our radiation measurement was of high quality.

We are not aware of a predictive model for changes in the incoming shortwave radiation $\Delta K_\downarrow$ in relation to ΔT_a. Our observations indicated a positive correlation between $\Delta K_\downarrow$ and ΔT_a, with a slope of 7.7 W m^{-2} K^{-1} (Figure 7d). According to the global analysis by Fildier and Collins (2015), the global mean clear-sky shortwave radiation at the surface should decline with climate warming due to more water vapor in the atmosphere. The opposite result observed here suggests that the relationship between $\Delta K_\downarrow$ and ΔT_a may vary with spatial and temporal scales.

In Figure 7, we did not show the albedo change versus temperature change, because Lake Taihu is ice free throughout the year. In midlatitude to high-latitude lakes, the annual mean albedo should decrease with increasing temperature due to the shortening of ice period (W. Wang et al., 2018). In other words, for lakes in cold climates, albedo change may play an important role in the lake energy budget.

The effect of future temperature changes on lake evaporation can be roughly predicted according to equation 3. With rising temperatures, the energy input terms $\Delta L_\downarrow$ and $\Delta K_\downarrow$ were shown to increase at rates of 7.4 and 7.7 W m^{-2} K^{-1}, respectively, and the outgoing longwave term $\Delta L_\uparrow$ to increase at a rate of 5.5 W m^{-2} K^{-1}. Furthermore, the $\Delta\beta$ term in equation 3 was equal to 1.6 W m^{-2} K^{-1} using the mean R_n and β (Table S1). The overall effect of rising temperature is equivalent to a rate of latent heat flux increase of 11.2 W m^{-2} K^{-1} or 13% K^{-1} (we have omitted the albedo change in this calculation). This rate of increase is greater than the temperature sensitivity of the global lake evaporation (4% K^{-1}; W. Wang et al., 2018) or

global Earth's surface evaporation (1 to 3% K^{-1}; Kirtman et al., 2013). The large $K_\downarrow$ change appears to be the main reason for this discrepancy. If we set $\Delta K_\downarrow$ to 0, we would obtain a lower evaporation temperature sensitivity of about 4% K^{-1}. Regardless of the $K_\downarrow$ trend, our results strongly imply that warming should enhance the evaporation of this lake.

The results of the correlation and the attribution analyses presented in the previous section showed that temperature as a nonenergy variable was not the main driver of the observed interannual variability in E. In this section, however, temperature was used as an independent variable to make prediction of future E change. This apparent contradiction can be understood from two different perspectives. The first perspective is theoretical, emphasizing the fact that evaporation is a process that consumes energy and therefore can be constrained by the energy balance principle. The second perspective is practical, requiring functional relationships to make prediction using easily measurable variables such as air temperature. Our approach is similar to that commonly used in studies of the global hydrological cycle in a warming climate. In those studies, changes in global evaporation and precipitation are constrained by the surface (e.g., Andrews et al., 2009) or the atmospheric energy balance (e.g., Myhre et al., 2017) to gain a mechanistic understanding, and individual terms of the energy balance equations are expressed as functions of temperature change to help predict how global precipitation may intensify with rising temperatures (DeAngelis et al., 2015; Kleidon et al., 2015; Pendergrass & Hartmann, 2014).

While the attribution analysis and the PT model performance are based on the observational data, the validity of future prediction depends on the accuracy of the underlying assumptions, namely, the PT model for the lake Bowen ratio, the extension of the Brutsaert's (1975) clear-sky parameterization to all-sky conditions, the assumption that climate warming does not change the near-surface RH, and the approximation that the lake albedo does not change with temperature. The constant RH assumption has been confirmed at the global scale from observations and climate models (Kirtman et al., 2013). It is encouraging that this assumption combined with the Brutsaert parameterization can predict reasonably well the interannual variability of the incoming longwave radiation at a local site (Lake Taihu). Whether these assumptions are valid at other lake sites requires further investigation. Nevertheless, our study shows that they provide a useful reference frame for interpreting long-term lake evaporation data.

5. Summary of Findings

In this paper, we analyzed the interannual variability of lake evaporation observed at Lake Taihu with eddy covariance over a 7-year period (2011–2017). The key findings are as follows:

1. The results confirmed that the attribution method based on the surface energy balance principle (W. Wang et al., 2018) is a useful tool for diagnosing changes in local lake evaporation.
2. The key drivers of the change of lake evaporation were incoming longwave radiation $L_\downarrow$ and incoming shortwave radiation $K_\downarrow$. The lake E was higher in years with higher $L_\downarrow$ and $K_\downarrow$. The outgoing longwave radiation $L_\uparrow$ had an opposite effect, offsetting about half of the $K_\downarrow$ and $L_\downarrow$ contributions to the lake evaporation changes.
3. The PT model underestimated the annual E by 9.3%. Forcing good agreement with the observed E requires that the PT α be increased from the original value of 1.26 to 1.39.
4. Climate change in the future has several consequences for lake evaporation, including reduction in Bowen ratio with rising temperature according to the PT model, increase in $L_\downarrow$ due to water vapor buildup in the atmosphere, and increase in $L_\uparrow$ due to warming of the lake water. Our results show that the interannual changes in these energy terms are predictable as functions of the temperature change. We found that Brutsaert's (1975) parameterization for atmospheric emissivity can be used to predict interannual changes in $L_\downarrow$.

References

Andrews, T., Forster, P. M., & Gregory, J. M. (2009). A surface energy perspective on climate change. *Journal of Climate*, *22*, 2557–2570. https://doi.org/10.1175/2008JCLI2759.1

Assouline, S., Li, D., Tyler, S., Tanny, J., Cohen, S., Bou-Zeid, E., et al. (2016). On the variability of the Priestley-Taylor coefficient over water bodies. *Water Resources Research*, *52*, 150–163. https://doi.org/10.1002/2015WR017504

Bello, R., & Smith, J. D. (1990). The effect of weather variability on the energy balance of a lake in the Hudson bay lowlands. *Canada Aric and Alpine Research*, *22*(1), 98–107. https://doi.org/10.2307/1551724

Blanken, P. D., Black, T. A., Yang, P. C., Newmann, H. H., Nesic, Z., Staebler, R., et al. (1997). Energy balance and canopy conductance of a boreal aspen forest: Partitioning overstory and understory components. *Journal of Geophysical Research*, *102*(D24), 28,915–28,927. https://doi.org/10.1029/97JD00193

Blanken, P. D., Rouse, W. R., Culf, A. D., Spence, C., Boudreau, L. D., Jasper, J. N., et al. (2000). Eddy covariance measurements of evaporation from Great Slave Lake, Northwest Territories, Canada. *Water Resources Research*, *36*(4), 1069–1077. https://doi.org/10.1029/1999WR900338

Blanken, P. D., Rouse, W. R., & Schertzer, W. M. (2003). Enhancement of evaporation from a large northern lake by the entrainment of warm, dry air. *Journal of Hydrometeorology*, *4*(4), 680–693. https://doi.org/10.1175/1525-7541(2003)004<0680:EOEFAL>2.0.CO;2

Blanken, P. D., Spence, C., Hedstrom, N., & Lenters, J. D. (2011). Evaporation from Lake Superior: 1. Physical controls and processes. *Journal of Great Lakes Research*, *37*(4), 707–716. https://doi.org/10.1016/j.jglr.2011.08.009

Bouin, M. N., Caniaux, G., Traullé, O., Legain, D., & Le Moigne, P. (2012). Long-term heat exchanges over a Mediterranean lagoon. *Journal of Geophysical Research*, *117*, D23104. https://doi.org/10.1029/2012JD017857

Brutsaert, W. (1975). On a derivable formula for long-wave radiation from clear skies. *Water Resources Research*, *11*, 742–744. https://doi.org/10.1029/WR011i005p00742

Brutsaert, W. (1982). *Evaporation into the atmosphere: Theory, history and applications*. Dordrecht, Holland: D. Reidel Publishing Co.

Brutsaert, W., & Parlange, M. B. (1998). Hydrologic cycle explains the evaporation paradox. *Nature*, *396*(6706), 30. https://doi.org/10.1038/23845

de Bruin, H. A. R., & Keijman, J. Q. (1979). The Priestley-Taylor evaporation model applied to a large, shallow lake in The Netherlands. *Journal of Applied Meteorology*, *18*, 898–903. https://doi.org/10.1175/1520-0450(1979)018<0898:TPTEMA>2.0.CO;2

DeAngelis, A. M., Qu, X., Zelinka, M. D., & Hall, A. (2015). An observational radiative constraint on hydrologic cycle intensification. *Nature*, *528*(7581), 249–253. https://doi.org/10.1038/nature15770

Deng, B., Liu, S., Xiao, W., Wang, W., Jin, J., & Lee, X. (2013). Evaluation of the CLM4 lake model at a large and shallow freshwater lake. *Journal of Hydrometeorology*, *14*, 636–649. https://doi.org/10.1175/JHM-D-12-067.1

Du, Q., Liu, H. Z., Liu, Y., Wang, L., Xu, L. J., Sun, J. H., & Xu, A. L. (2018). Factors controlling evaporation and the CO_2 flux over an open water lake in southwest of China on multiple temporal scales. *International Journal of Climatology*, *38*(13), 4723–4739. https://doi.org/10.1002/joc.5692

Feng, J. W., Liu, H. Z., Sun, J. H., & Wang, L. (2016). The surface energy budget and interannual variation of the annual total evaporation over a highland lake in Southwest China. *Theoretical and Applied Climatolology*, *126*(1-2), 303–312. https://doi.org/10.1007/s00704-015-1585-9

Fildier, B., & Collins, W. D. (2015). Origins of climate model discrepancies in atmospheric shortwave absorption and global precipitation changes. *Geophysical Research Letters*, *42*, 8749–8757. https://doi.org/10.1002/2015GL065931

Franz, D., Mammarella, I., Boike, J., Kirillin, G., Vesala, T., Bornemann, N., et al. (2018). Lake-atmosphere heat flux dynamics of a thermokarst lake in arctic Siberia. *Journal of Geophysical Research: Atmospheres*, *123*, 5222–5239. https://doi.org/10.1029/2017JD027751

Friedrich, K., Grossman, R. L., Huntington, J., Blanken, P. D., Lenters, J., Holman, K. D., et al. (2018). Reservoir evaporation in the western United States: Current science, challenges, and future needs. *Bulletin of the American Meteorological Society*, *99*(1), 167–187. https://doi.org/10.1175/BAMS-D-15-00224.1

Gallego-Elvira, B., Baille, A., Martín-Górriz, B., & Martínez-Álvarez, V. (2010). Energy balance and evaporation loss of an agricultural reservoir in a semi-arid climate (south-eastern Spain). *Hydrological Processes*, *24*, 758–766. https://doi.org/10.1002/hyp.7520

Garratt, J. R. (1994). *The atmospheric boundary layer*. Oxford: Elsevier.

Guo, X., Liu, H., & Yang, K. (2015). On the application of the Priestley-Taylor relation on sub-daily time scales. *Boundary-Layer Meteorology*, *156*(3), 489–499. https://doi.org/10.1007/s10546-015-0031-y

Guo, Y., Zhang, Y., Ma, N., Xu, J., & Zhang, T. (2019). Long-term changes in evaporation over Siling Co Lake on the Tibetan Plateau and its impact on recent rapid lake expansion. *Atmospheric Research*, *216*, 141–150. https://doi.org/10.1016/j.atmosres.2018.10.006

Hu, C., Wang, Y., Wang, W., Liu, S., Piao, M., Xiao, W., & Lee, X. (2017). Trends in evaporation of a large subtropical lake. *Theoretical and Applied Climatology*, *129*(1-2), 159–170. https://doi.org/10.1007/s00704-016-1768-z

Hunter, T. S., Clites, A. H., Campbell, K. B., & Gronewold, A. D. (2015). Development and application of a North American Great Lakes hydrometeorological database—Part I: Precipitation, evaporation, runoff, and air temperature. *Journal of Great Lakes Research*, *41*(1), 65–77. https://doi.org/10.1016/j.jglr.2014.12.006

Kirtman, B., Power, S. B., Adedoyin, J. A., Boer, G. J., Bojariu, R., Camilloni, I., et al. (2013). Near-term climate change: Projections and predictability. In T. F. Stocker, et al. (Eds.), *Climate Change 2013: The physical science basis. Contribution of Working Group I to the Fifth Assessment Report of the Intergovernmental Panel on Climate Change* (pp. 953–1028). Cambridge, United Kingdom and New York, NY, USA: Cambridge University Press.

Kleidon, A., Kravitz, B., & Renner, M. (2015). The hydrological sensitivity to global warming and solar geoengineering derived from thermodynamic constraints. *Geophysical Research Letters*, *41*, 138–144. https://doi.org/10.1002/2014GL062589

Lazhu, Y. K., Wang, J., Lei, Y., Chen, Y., Zhu, L., Ding, B., & Qin, J. (2016). Quantifying evaporation and its decadal change for Lake Nam Co, central Tibetan Plateau. *Journal of Geophysical Research: Atmospheres*, *121*, 7578–7591. https://doi.org/10.1002/2015JD024523

Lee, X., Finnigan, J., & Paw, U. K. T. (2004). Coordinate systems and flux bias error. In X. Lee, W. Massman, B. Law (Eds.). *Handbook of micrometeorology: a guide for surface flux measurement andanalysis* (pp. 33–66). Dordrecht: Kluwer.

Lee, X., Goulden, M. L., Hollinger, D. Y., Barr, A., Black, T. A., Bohrer, G., et al. (2011). Observed increase in local cooling effect of deforestation at higher latitudes. *Nature*, *479*(7373), 384–387. https://doi.org/10.1038/nature10588

Lee, X., Liu, S., Xiao, W., Wang, W., Gao, Z., Cao, C., et al. (2014). The Taihu Eddy Flux Network: An observational program on energy, water and greenhouse gas fluxes of a large freshwater lake. *Bulletin of the American Meteorological Society*, *95*(10), 1583–1594. https://doi.org/10.1175/BAMS-D-13-00136.1

Lee, X., & Massman, W. (2011). A perspective on thirty years of the Webb, Pearman and Leuning density corrections. *Boundary-Layer Meteorology*, *139*(1), 37–59. https://doi.org/10.1007/s10546-010-9575-z

Lenters, J. D., Kratz, T. K., & Bowser, C. J. (2005). Effects of climate variability on lake evaporation: Results from a long-term energy budget study of Sparkling Lake, northern Wisconsin (USA). *Journal of Hydrology*, *308*, 168–195. https://doi.org/10.1016/j.jhydrol.2004.10.028

Liu, H., Blanken, P. D., Weidinger, T., Nordbo, A., & Vesala, T. (2011). Variability in cold front activities modulating cool-season evaporation from a southern inland water in the USA. *Environmental Research Letters*, *6*, 024022. http://doi.org/10.1088/1748-9326/6/2/024022

Liu, H., Zhang, Y., Liu, S., Jiang, H., Li, S., & Williams, Q. L. (2009). Eddy covariance measurements of surface energy budget and evaporation in a cool season over southern open water in Mississippi. *Journal of Geophysical Research*, *114*, D04110. https://doi.org/10.1029/2008JD010891

Ma, N., Szilagyi, J., Niu, G. Y., Zhang, Y., Zhang, T., Wang, B., & Wu, Y. (2016). Evaporation variability of Nam Co Lake in the Tibetan Plateau and its role in recent rapid lake expansion. *Journal of Hydrology*, *537*, 27–35. https://doi.org/10.1016/j.jhydrol.2016.03.030

McGloin, R., McGowan, H., & McJannet, D. (2015). Effects of diurnal, intra-seasonal and seasonal climate variability on the energy balance of a small subtropical reservoir. *International Journal of Climatology*, *35*, 2308–2325. https://doi.org/10.1002/joc.4147

McJannet, D., Cook, F., McGloin, R., McGowan, H., Burn, S., & Sherman, B. (2013). Long-term energy flux measurements over an irrigation water storage using scintillometry. *Agricultural and Forest Meteorology*, *168*, 93–107. https://doi.org/10.1016/j.agrformet.2012.08.013

Monteith, J. L., & Unsworth, M. H. (1990). *Principles of environmental physics: Plants, animals, and the atmosphere*. San Diego, CA: Elsevier.

Myhre, G., Forster, P. M., Samset, B. H., Hodnebrog, Ø., Sillmann, J., & Aalbergsjø, S. G. (2017). PDRMIP: A precipitation driver and response model intercomparison project—Protocol and preliminary results. *Bulletin of the American Meteorological Society*, *98*, 1185–1198. https://doi.org/10.1175/BAMS-D-16-0019.1

Nordbo, A., Launiainen, S., Mammarella, I., Leppäranta, M., Huotari, J., Ojala, A., & Vesala, T. (2011). Long-term energy flux measurements and energy balance over a small boreal lake using eddy covariance technique. *Journal of Geophysical Research*, *116*, D02119. https://doi.org/10.1029/2010JD014542

Pendergrass, A. G., & Hartmann, D. L. (2014). The atmospheric energy constraint on global-mean precipitation change. *Journal of Climate*, *27*(2), 757–768. https://doi.org/10.1175/JCLI-D-13-00163.1

Peterson, T. C., Golubev, V. S., & Groisman, P. Y. (1995). Evaporation losing its strength. *Nature*, *377*(6551), 687–688. https://doi.org/10.1038/377687b0

Priestley, C. H. B., & Taylor, R. J. (1972). On the assessment of surface heat flux and evaporation using large-scale parameters. *Monthly Weather Review*, *100*(2), 81–92. https://doi.org/10.1175/1520-0493(1972)100<0081:OTAOSH>2.3.CO;2

Richter, I., & Xie, S.-P. (2008). Muted precipitation increase in global warming simulations: A surface evaporation perspective. *Journal of Geophysical Research*, *113*, D24118. https://doi.org/10.1029/2008JD010561

Roderick, M. L., & Farquhar, G. D. (2002). The cause of decreased pan evaporation over the past 50 years. *Science*, *298*(5597), 1410–1411. https://doi.org/10.1126/science.1075390-a

Rouse, W. R., Oswald, C. M., Binyamin, J., Blanken, P. D., Schertzer, W. M., & Spence, C. (2003). Interannual and seasonal variability of the surface energy balance and temperature of central Great Slave Lake. *Journal of Hydrometeorology*, *4*, 720–730. https://doi.org/10.1175/1525-7541(2003)004<0720:IASVOT>2.0.CO;2

Stewart, R. B., & Rouse, W. R. (1976). A simple method for determining the evaporation from shallow lakes and ponds. *Water Resources Research*, *12*(4), 623–628. https://doi.org/10.1029/WR012i004p00623

Subin, Z. M., Riley, W. J., & Mironov, D. (2012). An improved lake model for climate simulations: Model structure, evaluation, and sensitivity analyses in CESM1. *Journal of Advances in Modeling Earth Systems*, *4*, M02001. https://doi.org/10.1029/2011MS000072

Tanny, J., Cohen, S., Berger, D., Teltch, B., Mekhmandarov, Y., Bahar, M., et al. (2011). Evaporation from a reservoir with fluctuating water level: Correcting for limited fetch. *Journal of Hydrology*, *404*(3-4), 146–156. https://doi.org/10.1016/j.jhydrol.2011.04.025

Twine, T. E., Kustas, W. P., Norman, J. M., Cook, D. R., Houser, P. R., Meyer, T. P., et al. (2000). Correcting eddy-covariance flux underestimates over a grassland. *Agricultural and Forest Meteorology*, *103*(3), 279–300. https://doi.org/10.1016/S0168-1923(00)00123-4

Wang, J., & Bras, R. L. (1999). Ground heat flux estimated from surface soil temperature. *Journal of Hydrology*, *216*, 214–226. https://doi.org/10.1016/S0022-1694(99)00008-6

Wang, T., Zhang, J., Sun, F., & Liu, W. (2017). Pan evaporation paradox and evaporative demand from the past to the future over China: A review. *Wiley Interdisciplinary Reviews Water*, *4*, e1207. https://doi.org/10.1002/wat2.1207

Wang, W., Lee, X., Xiao, W., Liu, S., Schultz, N., Wang, Y., et al. (2018). Global lake evaporation accelerated by changes in surface energy allocation in a warmer climate. *Nature Geoscience*, *11*(6), 410–414. https://doi.org/10.1038/s41561-018-0114-8

Wang, W., Xiao, W., Cao, C., Gao, Z., Hu, Z., Liu, S., et al. (2014). Temporal and spatial variations in radiation and energy balance across a large freshwater lake in China. *Journal of Hydrology*, *511*, 811–824. https://doi.org/10.1016/j.jhydrol.2014.02.012

Webb, E. K., Pearman, G. I., & Leuning, R. (1980). Correction of flux measurements for density effects due to heat and water vapour transfer. *Quarterly Journal of the Royal Meteorological Society*, *106*(447), 85–100. https://doi.org/10.1002/qj.49710644707

Woolway, R. I., Verburg, P., Lenters, J. D., Merchant, C. J., Hamilton, D. P., Brookes, J., et al. (2018). Geographic and temporal variations in turbulent heat loss from lakes: A global analysis across 45 lakes. *Limnology and Oceanography*, *63*(6), 2436–2449. https://doi.org/10.1002/lno.10950

Xiao, K., Griffis, T. J., Baker, J. M., Bolstad, P. V., Erickson, M. D., Lee, X., et al. (2018). Evaporation from a temperate closed-basin lake and its impact on present, past, and future water level. *Journal of Hydrology*, *561*, 59–75. https://doi.org/10.1016/j.jhydrol.2018.03.059

Xiao, W., Liu, X., Wang, W., Yang, D., Xu, J., Cao, C., et al. (2013). Transfer coefficient of momentum, heat and water vapour in the atmospheric surface layer of a large freshwater lake. *Boundary-Layer Meteorology*, *148*(3), 479–494. https://doi.org/10.1007/s10546-013-9827-9

Yang, Y., & Roderick, M. L. (2018). Radiation, surface temperature and evaporation over wet surface. *Quarterly Journal of the Royal Meteorological Society*, *145*, 1118–1129. https://doi.org/10.1002/qj.3481

Zhao, X., & Liu, Y. (2018). Variability of surface heat fluxes and its driving forces at different time scales over a large ephemeral lake in China. *Journal of Geophysical Research: Atmospheres*, *123*, 4939–4957. https://doi.org/10.1029/2017JD027437